Obtaining Frequency Markers of Variable Separation with a Spherical Mirror Fabry-Perot Interferometer

Dmitry Budker[a)]

Department of Physics, University of California, Berkeley, Berkeley, CA 94720-7300, USA and Nuclear Science Division, Lawrence Berkeley National Laboratory, Berkeley, California 94720, USA

Simon M. Rochester

Department of Physics, University of California, Berkeley, Berkeley, CA 94720-7300, USA

Valeriy V. Yashchuk

Department of Physics, University of California, Berkeley, Berkeley, CA 94720-7300, USA and B.P.Konstantinov Petersburg Nuclear Physics Institute, Gatchina, Russia 188350

ABSTRACT

A compact ($L \approx 5\ cm$) spherical Fabry-Perot interferometer with adjustable mirror spacing is used to produce interference fringes with frequency separation $(c/2L)/N$, $N \lesssim 20$. These fringes are used as frequency markers in a Doppler-free saturation spectroscopy experiment. The conditions for observation of the fringes are discussed in terms of the eigenmodes of the cavity with high transverse indices.

PACS numbers: 42.62.Fi, 07.60.Ly, 01.50.Pa.

1 Introduction

Spherical mirror Fabry-Perot interferometers in the confocal configuration (see e.g. Refs. 1, 2) have many advantages over flat mirror interferometers. They are used in a variety of spectroscopic applications, including laser spectrum analysis and for generating frequency markers for laser frequency scans (see e.g. Ref. 3). In recent years, inexpensive home-made devices have found broad application both in research and instruction laboratories. In a typical design[4] (see Fig.1), the body of the interferometer is constructed of two fine-threaded invar (a low thermal expansion alloy) pipes. One pipe threads into the other allowing accurate adjustment of the mirror separation necessary for achieving the confocal condition (separation between the mirrors equal to the radius of curvature for a symmetric interferometer). A standard concave mirror (intensity reflectivity $\mathcal{R} = 95 - 98\%$, radius of curvature $R = 5\ cm$) is glued directly to one of the pipes. The second identical mirror is glued to a piezo-ceramic hollow cylinder, which, in turn, is glued to the second invar pipe. Application of voltage between the walls of the piezo-ceramic tube displaces the mirror, providing frequency tuning of the interferometer, typically, by several free spectral ranges (FSR=frequency interval between adjacent transmission peaks) per $100\ V$. Adjustment of the average mirror separation to achieve the confocal condition (tolerance $\sim 10^{-2}\ mm$) is accomplished while scanning either the interferometer or the laser and minimizing the width of the observed transmission peaks. Once the confocal separation between the mirrors is found, it can be locked by tightening the retaining nut.

Such a device, when the separation between the mirrors is adjusted to specific values different from the separation corresponding to the confocal condition, can be used to generate fringes that are separated by $(c/2L)/N$, where c is the speed of light, L is the separation between the mirrors, and $N > 1$ is an integer ($N = 2$ for a confocal interferometer). In our experiments, we produced well resolved fringes with N up to ≈ 20. Although the finesse of the interferometer (the ratio of FSR to the transmission peak width at half maximum) and the peak transmission decrease with N, the ability to produce fringes with small adjustable FSR allows the use of a single compact device in place of multiple interferometers of much greater length. This is useful, for example, in such applications where one needs frequency markers for a laser scan over narrow spectral features (such as Doppler-free saturation spectroscopy lines, see. e.g. Ref. 4).

2 Transverse modes in a spherical mirror interferometer

The method of obtaining fringes with large N takes advantage of the fact that without mode-matching (i.e. preferential coupling into a single mode), one typically excites many transverse modes of the interferometer. For example, for the interferometer used in the present work ($R = 5\ cm$; $L \approx 5\ cm$), the size of the fundamental transverse mode on a mirror is $w \approx (L\lambda/\pi)^{1/2} \approx 0.1\ mm$, where $\lambda = 780\ nm$ is the wavelength of the light. Since the width of higher transverse

modes with index m is roughly $\sqrt{m} \cdot w$ (see e.g. Ref. 2), if we illuminate the input mirror with a laser beam, for example, of a size $\sim 1\ mm$, we expect that transverse modes with $m < m_{max} \sim 100$ will be excited (and even higher modes if the beam is offset from the axis). Similarly, we have $n < m_{max}$ for the other transverse direction.

It is well-known that, as one adjusts mirror spacing in the spherical interferometer approaching the confocal condition, the frequencies of the transverse modes all become nearly-degenerate with either the axial modes, or the "half axial modes."[2] This is illustrated in Fig. 2 which shows the interferometer transmission spectra at different mirror separations obtained by a straightforward model calculation[5] (including transverse modes with indices m, n corresponding to the two transverse directions). Assuming phase shift per double pass of the length of the resonator[2] of:

$$\varphi(m+n, L) = 2\pi \left(\frac{2L}{\lambda} - \frac{(m+n+1)\arccos\left[1 - \frac{L}{R}\right]}{\pi} \right), \tag{1}$$

one calculates the output signal of the interferometer as a sum of Airy functions for each mode:

$$S(L) = \sum_{m+n} \frac{W(m+n)}{1 + F \cdot \sin^2\left[\varphi(m+n, L)/2\right]}. \tag{2}$$

Here $F = 4\mathcal{R}/(1-\mathcal{R})^2$ (the factor F is related to *reflectivity finesse* $\mathcal{F}$ according to $\mathcal{F} = \pi\sqrt{F}/2$, and the factors $W(m+n)$ describe the relative weight of various transverse modes. These factors can be found by a straightforward expansion of the input field in the Hermite-gaussian basis (see e.g. Chapter 17.5 of Ref. 2). We find that any approximation assuming a gradual decrease of the W-

factors for modes with m, n up to m_{max}, reproduces the essential features of the observed transmission patterns.

In addition to the primary "resonance," corresponding to the confocal condition where every other transverse mode is degenerate with a longitudinal mode and the frequency interval between adjacent transverse modes is a half of the axial mode interval $(c/2L)$, there are additional "resonances"[6] where the frequency interval between adjacent modes is $(c/2L)/N,\ N > 2$, which correspond to the degeneracy (Fig. 3):

$$\nu(q, k + N) = \nu(q + l, k) \tag{3}$$

Here we label modes by a pair of indices, the first of which is the axial index, and the second is the combined transverse index, $k = m + n$, and l is an integer. Since the mode frequencies are given by (see e.g. Eq.(1) and a discussion in Ref. 2):

$$\nu(q, k) = \frac{c}{2L}\left(q + \frac{k+1}{\pi}\arccos\left[1 - \frac{L}{R}\right]\right), \tag{4}$$

one obtains the resonance condition as

$$\frac{L}{R} = 1 - \cos\left[\frac{l\pi}{N}\right];\quad l, N \text{ mutually prime, } l < N. \tag{5}$$

The additional conditions are added to avoid double counting resonances with higher degeneracies. The location of the solutions of Eq.(5) is shown in Fig. 4.

3 Experiment and limitations of the technique

Examples of experimental transmission patterns of an interferometer with mirror separations in the vicinity of a confocal resonance and a resonance with $N = 15$ is given in Figures 5 and 6. These Figures also show the Doppler-limited absorption spectrum of the Rb D2 line (Fig. 5 c) and a recording of the Doppler-free saturated absorption signal (Fig. 6 a) with a considerably smaller scan range. The $N = 15$ fringes are useful as frequency markers in the latter case.

Since a smaller number of modes are degenerate between each other for $N > 2$ compared to the confocal case, the peak transmission of the interferometer is reduced, roughly as $2/N$. The widths of the transmission peaks corresponding to a given mode are mostly determined by the mirrors' reflectivity and do not change with N. Thus, the effective finesse of the device also scales as $2/N$.

4 Acknowledgements

The authors are grateful to A. Vaynberg for manufacturing parts of the interferometers, K. Kerner for technical assistance, and to D. DeMille, A. E. Siegman, B. Ya. Zel'dovich, and M. Zolotorev for helpful discussions. This work is supported by ONR grant (N00014-97-1-0214), NSF (grant PHY-9733479), and by the U.S. Department of Energy under Contract No. DE-AC03-76SF00098 through the LBNL Nuclear Sciences Division.

[a)] E-mail: budker@socrates.Berkeley.edu

REFERENCES

[1] J. M. Vaughan, *The Fabry-Perot interferometer. History, theory, practice and applications* (Adam Hilger, Bristol and Philadelphia, 1989); G. Hernandez, *Fabry-Perot interferometers* (Cambridge University Press, Cambridge, New York, 1988).

[2] A. E. Siegman, *Lasers*, University Science Books (Mill Valley, California, 1986).

[3] W. Demtröder, *Laser specroscopy* (Springer-Verlag, Berlin, Heidelberg, New-York, 1998).

[4] D. Budker, D. J. Orlando, and V. Yashchuk, Am. J. Phys. **67**, 584 (1999).

[5] We use the paraxial approximation and assume that L is effectively the same for all modes. In order to ensure sufficiently close equality of the spacing between transverse modes, we require that (see e.g. Ref. 3) $\rho^4/R^3 < \lambda/100$, where ρ is a typical size characterizing the width and offset from the axis of the input laser beam. This means that ρ is limited to $\sim 1\ mm$ for the interferometers used in this work. Larger beam sizes and offsets lead to broader and asymmetric transmission peaks.

[6] We emphasize that observation of multiple modes outside the confocal condition has been described by many authors (see e.g. R. A. Boyd, J. L. Bliss, and K. G. Libbrecht, Am. J. Phys. **64**, 1109 (1996)), but they are usu-

ally considered a useless "jumble." We point out, however, that when the resonance condition is satisfied, the observed pattern may be quite regular (Figures 5,6) and useful for applications. The problem has also been analyzed in the ray-tracing approach in D. Herriott, H. Kogelnik, and R. Kompner, Appl. Opt. **3**(4), 523 (1964) (see also J. R. Johnson, Appl. Opt. **7**(6), 1061 (1968)). In that work, the relation of the extra cavity resonances to the appearance of closed ray paths and applications to laser resonators and absorption cells are discussed.

CAPTIONS

Figure 1: Schematic of a Fabry-Perot interferometer with spherical mirrors and adjustable mirror spacing.

Figure 2: Calculated transmission spectra of the interferometer close to the confocal separation (a), and close to a resonance with $N = 15$ (b). Note the difference in FSR in the two cases, relative transmission amplitudes, and comparable sensitivity to adjustment of the mirror separation L.

Figure 3: A schematic (analogous to Fig. 19.16 in Ref. 2) illustrating as an example the origin of the additional resonance with $N = 5$. The figure is drawn assuming constant mirror separation L and variable radius of curvature R. This allows to trace the evolution of the relative mode positions as a function of L/R. The resonance occurs when the frequency of the mode $(q-2, 5)$ becomes degenerate with that of the mode $(q, 0)$. Transverse modes are shown with lines of different sizes to distinguish them between each other.

Figure 4: Location of the solutions of Eq.(5). This plot can be used for choosing appropriate mirror separation for a desired value of N.

Figure 5: a) Recording of a transmission pattern of the interferometer with the mirror spacing adjusted to $L = 5.000(10)$ cm corresponding to the confocal

condition. b) Same with the mirror spacing adjusted to $L = 4.485(10)\ cm$ close to a resonance with $N = 15$ in Eqs.(4,5). c) Doppler-limited transmission spectrum of the $D2$ line in rubidium.

Figure 6: a) Recording of a Doppler-free saturated absorption spectrum with a procedure described in Ref. 4. The lines are labeled by the values of the total upper state angular momentum F'. C/O designates cross-over resonances. b). Same as Fig. 2b but with expanded horizontal scale. This illustrates the utility of the device for providing frequency markers for high-resolution scans. The residual asymmetry of the peaks is presumably due to imperfect adjustment of L to the resonance value.

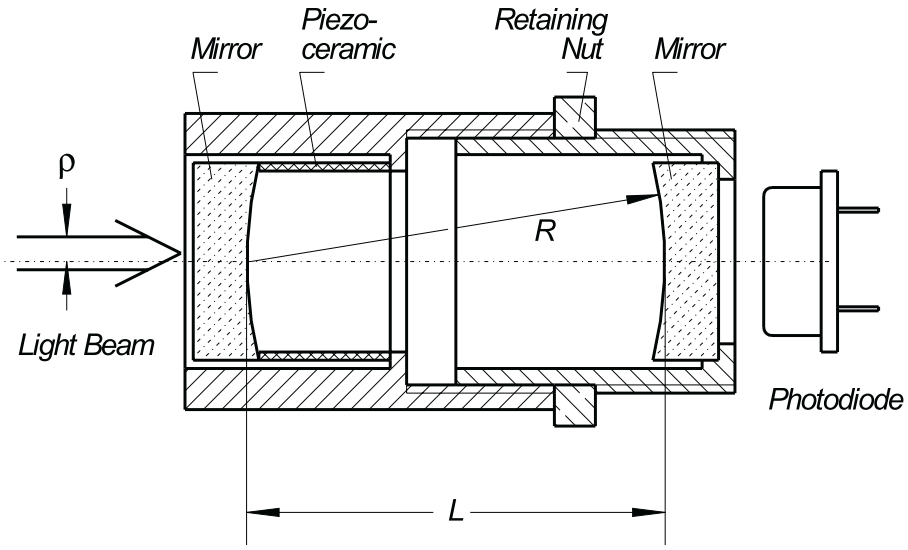

Figure 1: D. Budker et al "Variable Free Spectral Range..."

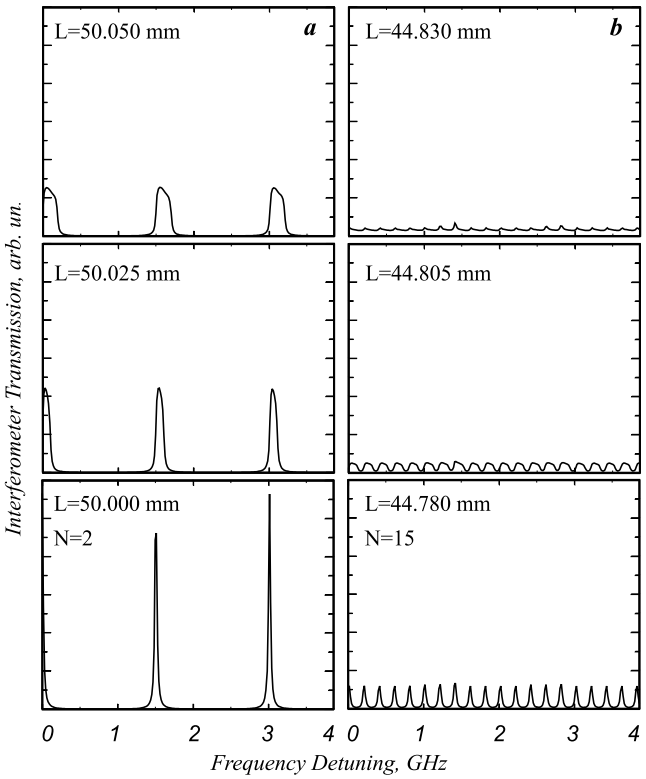

Figure 2: D. Budker et al "Variable Free Spectral Range..."

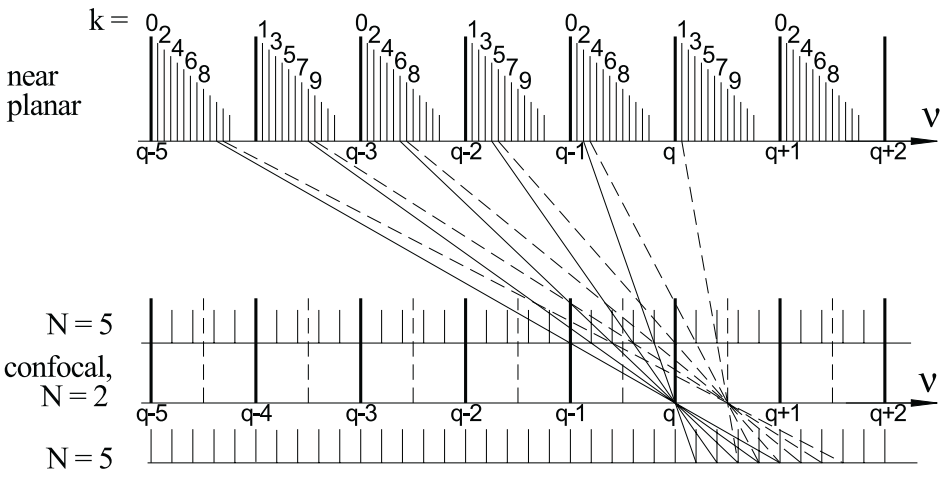

Figure 3: D. Budker et al "Variable Free Spectral Range..."

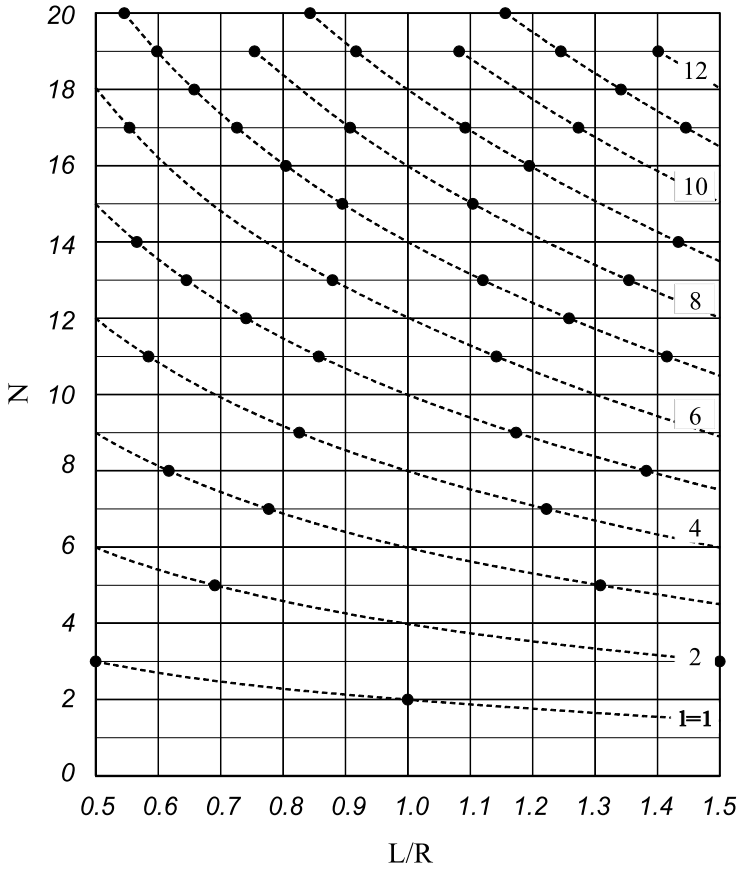

Figure 4: D. Budker et al "Variable Free Spectral Range..."

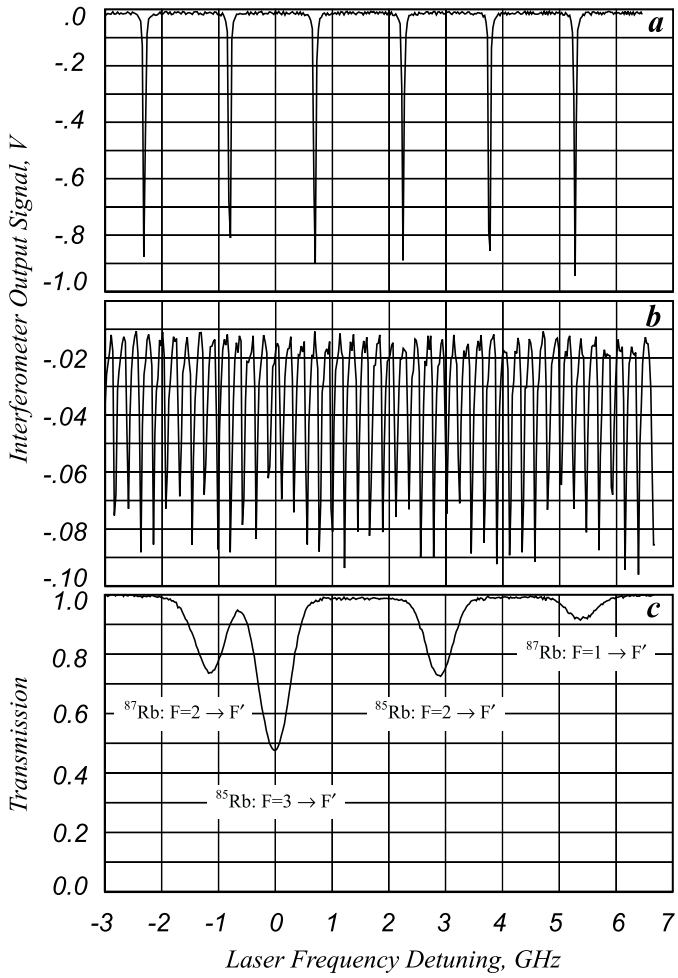

Figure 5: D. Budker et al "Variable Free Spectral Range..."

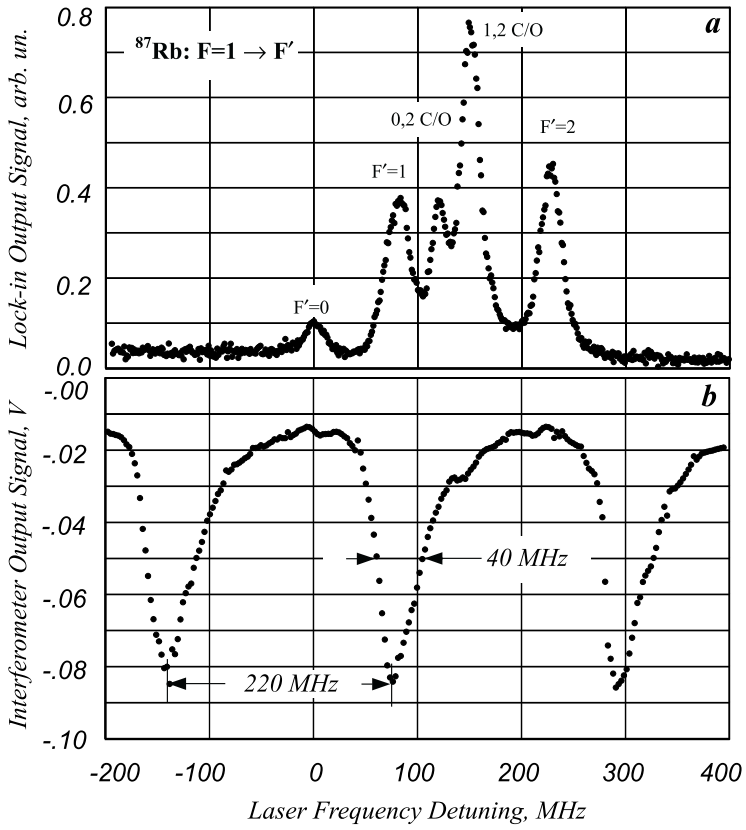

Figure 6: D. Budker et al "Variable Free Spectral Range..."